Chalcogenide Letters Vol. 18, No. 10, October 2021, p. 589 - 599

Magnetic and optical characteristics of Fe doped $SrTiO_3$ perovskite compound: a first principle study

H. Shafique[a], S. A. Aldaghfag[b] , M. Kashif[c], M. Zahid[d] , M.Yaseen[a*], J. Iqbal[d], Misbah[d], R. Neffati[e,f]

[a]*Spin-Optoelectronics and Ferro-Thermoelectric (SOFT) Materials and Devices Laboratory, Department of Physics, University of Agriculture, Faisalabad 38040, Pakistan*

[b]*Department of Physics, College of Sciences, Princess Nourah bint Abdulrahman University (PNU), Riyadh 11671, Saudi Arabia*

[c]*Physics Department, Govt College University Faisalabad (GCUF), Allama Iqbal Road, Faisalabad 38000, Pakistan*

[d]*Department of Chemistry, University of Agriculture, Faisalabad 38040, Pakistan*

[e]*Department of Physics - Faculty of Science - King Khalid University, P.O. Box 9004, Abha, Saudi Arabia*

Laboratory of Condensed Matter Physics, Department of Physics, Faculty of
[f]*Sciences of Tunis, University of Tunis El Manar, 1060 Tunis, Tunisia*

In this study, we theoretically probed the electronic, magnetic and optical characteristics of $Sr_{1-x}Fe_xTiO_3$ and $SrTi_{1-x}Fe_xO_3$ perovskite materials with the implementation of DFT based Wein2K code. In both doping atom is partially removed by (Fe) dopant. The substitution of Fe at A-site in $SrTiO_3$ consequences the half-metallic ferromagnetic (FHM) character, while the substitution of Fe at B-site in $SrTiO_3$ resulted into metallic character of the studied material. Moreover, In $Sr_{0.5}Fe_{0.5}TiO_3$ the local magnetic moment of Fe is slightly decreased, whereas in $SrTi_{0.5}Fe_{0.5}O_3$ the Fe magnetic moment is highly decreased from its free space value 4 μ_B. This reduction is due to *p-d* hybridization. In case of $Sr_{0.5}Fe_{0.5}TiO_3$, the exchange constants $N_0\alpha$ for *s-d* and $N_0\beta$ for *p-d* interaction are computed. The optical response of studied materials is described by jn.hat $Sr_{0.5}Fe_{0.5}TiO_3$ is a prominent candidate for spintronics applications.

(Received June 24, 2021; Accepted October 3, 2021)

Keywords: DFT, Half metallic, Magnetic moment, Optical properties

1. Introduction

Perovskite materials attracted attention of the material scientists due to their unique properties like semi-conductivity, ferroelectricity, ferromagnetism, structure phase transition, etc [1-4]. Strontium titanate ($SrTiO_3$) belongs to the ABO_3-type oxide perovskite materials. It reveals the mixed ionic-covalent bonding due to the nature of bond that lies between Sr-O (strongly covalent) and Ti-O (strongly ionic) [5]. At room temperature, $SrTiO_3$ is a paraelectric with a cubic phase structure. It undergoes structural phase transformation from high to low symmetry by varying temperature and have a melting temperature of 2350 K. $SrTiO_3$ possesses large dielectric constant (300) and has a large indirect energy gap of 3.2 eV that only absorbs the UV radiation which forms 4% of Sun radiations[6-9]. It has applications in field of magneto-optics, electrochemistry, microwaves, microelectronics, superconducting electronics and gas sensing [3, 10-12]. Moreover, $SrTiO_3$ exhibits multiferroic response, i.e. the coexistence of magnetism and ferroelectricity in a single phase of material [13-15]. Thus, it also has applications in spintronic and magnetic storage devices. Various attempts have been made to further enhance the physical characteristics of the perovskite materials. Among them, doping was assumed to be efficient approach for improving their properties. In case of strontium titanate (STO), the main criterion for a possible incorporation of Sr-site or Ti-site ions by impurity atoms should related with the ionic

* Corresponding author: myaseen_taha@yahoo.com
https://doi.org/10.15251/CL.2021.1810.589

radius of respective species. The foreign element with the oxidation state lower than the host atom behaves as acceptor (Fe^{3+}, Sc^{3+}, Na^{+1}),where as the higher oxidation state foreign element behaves as donor (Al^{3+}, La^{3+}, Nb^{5+}) [16]. Recent investigations revealed that some metals (Mg, Mn, Fe, Nb, Cr and Cu) and non-metals (N, C, S, B and P) doped and co-doped strontium titanate (STO) perovskite materials are effective way to improve the conductivity and photo-catalytic activity [17-23]. Zang et al. observed RT ferromagnetic response in Co-doped $SrTiO_3$ due to pure large spin configuration of cobalt [24]. Maikhuri et al. investigated Fe incorporated at A-site and B-site in barium titanate (BTO). It is found that the coercive field is increased by the incorporation of Fe at B-site, while saturation magnetization is enhanced by the incorporation of Fe at A-site in BTO samples [25]. It is deduced by surveying literature that there is no such data available which covers simultaneous study of Fe substituted at A/B- sites strontium titanate (STO).

In this work, we investigated the influence of partially substituted Fe at A- and B- site in $SrTiO_3$to study its electronic, magnetic and optical properties by using the FP-LAPW based Wein2K program.

2. Method of calculation

All the evaluations are performed by employing the Wein 2K software that is based on DFT under the framework of Full potential-LAPW approach [26, 27]. PBE+GGA scheme is implemented to analyze the exchange and correlation potential [28]. The Full potential-LAPW is one of the most efficient and reliable methodology in solving the Khon- Sham equation. In this approach, Muffin-Tin radii are employed for dividing the unit cell of crystal into two zones: (i) spherical zone (where the wave-function is assumed to be atomic like). (ii) Interstitial zone (where the wave-function is assumed to be plane wave). The cut-off energy is adjusted at -6 Ry which describes the separation between the core and valence electronic orbitals.The angular momentum (l_{max}) for MT-sphere is equal to 9. Moreover the product $R_{MT} \times K_{max}$= 6 eV is chosen for the plane wave expansion, where R_{MT} reveals the radii of the smallest MT-sphere and K_{max} reveals the highest K-vector. The R_{MT} values were taken as 2.50 for Sr, 2.50 for Fe, 1.67 for Ti and O atoms. The BZ-integrations in a grid of 10×10×10 meshes are sampled at 1000 k-points by using the Monkhorst-pack (MP) method [29]. The 35 K-points applied in the irreducible part of BZ.The $5s^2$ electrons of Sr, the $3d^{10}$, $4s^2$ electrons of Ti, the $2p^4$electrons of O and the $3d^6$ electrons of Fe are treated as valence electrons. The optical properties of the studied compounds are explained with respect to the complex dielectric function (DF) which consists of two parts: (i) real part $\varepsilon_1(\omega)$ and (ii) imaginary part $\varepsilon_2(\omega)$ [30]. The latter part is calculated from momentum matrix components and former part is attained from $\varepsilon_2(\omega)$ by employing the Kramer kronig transformation. From the knowledge DF ($\varepsilon(\omega) = \varepsilon_1(\omega) + i\varepsilon_2(\omega)$), all the other optical parameters are explained [31-32].

3. Results and discussions

3.1. Electronic Properties

The optimized structures of partially substituted Fe: $SrTiO_3$perovskite material (shown in Fig. 1) with an optimized computed lattice constant of 3.9803 A^o. The evaluated ground state energies in PM, AFM and FM phases are delineated in Fig. 2. It is observed that the studied materials are most stable in ferromagnetic (FM) state. In addition, the positive value of $\Delta E = E_{AFM} - E_{FM}$ confirms that the studied compounds have maximum stability in FM state. The detail discussion about the electronic properties are made into two sections.(i) For Fe doping at A-site in $SrTiO_3$, (ii) For Fe doping at B-site in $SrTiO_3$.

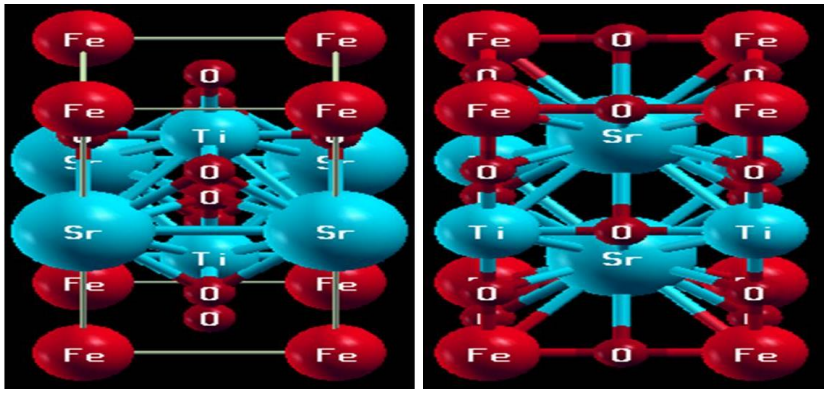

(a) (b)

Fig.1. The structures of (a) $Sr_{0.5}Fe_{0.5}TiO_3$ and (b) $SrTi_{0.5}Fe_{0.5}O_3$ compounds.

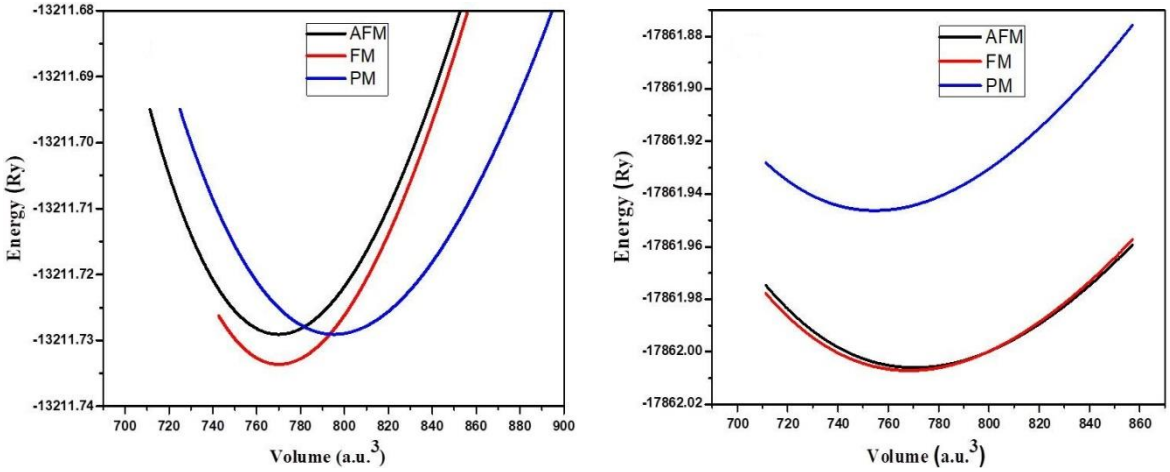

(a) (b)

Fig. 2. The spin dependent total energy vs. unit cell volume for ferromagnetic (FM), Antiferromagnetic (AFM) and paramagnetic (PM) states for (a) $Sr_{0.5}Fe_{0.5}TiO_3$ and(b) $SrTi_{0.5}Fe_{0.5}O_3$.

3.1.1. Electronic properties of $Sr_{0.5}Fe_{0.5}TiO_3$

Electronic band structure (BS) is used to demonstrate the electrons possible transitions in a material from top of valence band (VB) to lower of conduction band (CB) [33]. Fig.3 depicts the calculated electron BS in a highly symmetry lines of the BZ for both spin of Fe doping at Sr-site in $SrTiO_3$ ($Sr_{1-x}Fe_xTiO_3$ where x = 0.5). It is observed for the majority spin channel (up-spin) that the top of VB is situated at point M and the lowest of CB is situated at point Γ. This reveals that there is indirect (Γ-M) energy gap of 1.9 eV and material shows semiconducting response in the spin-up state. However, for the minority spin channel (down-spin) few VB cross the Fermi level (E_f) and reach the CB due to the addition of Fe-*d* orbital electrons.This indicates $Sr_{0.5}Fe_{0.5}TiO_3$ shows the metallic response in the spin-down state. Thus, $Sr_{0.5}Fe_{0.5}TiO_3$ material possesses the HMF character due to distinct behavior in spin-up state (semiconducting) and spin-down state (metallic).

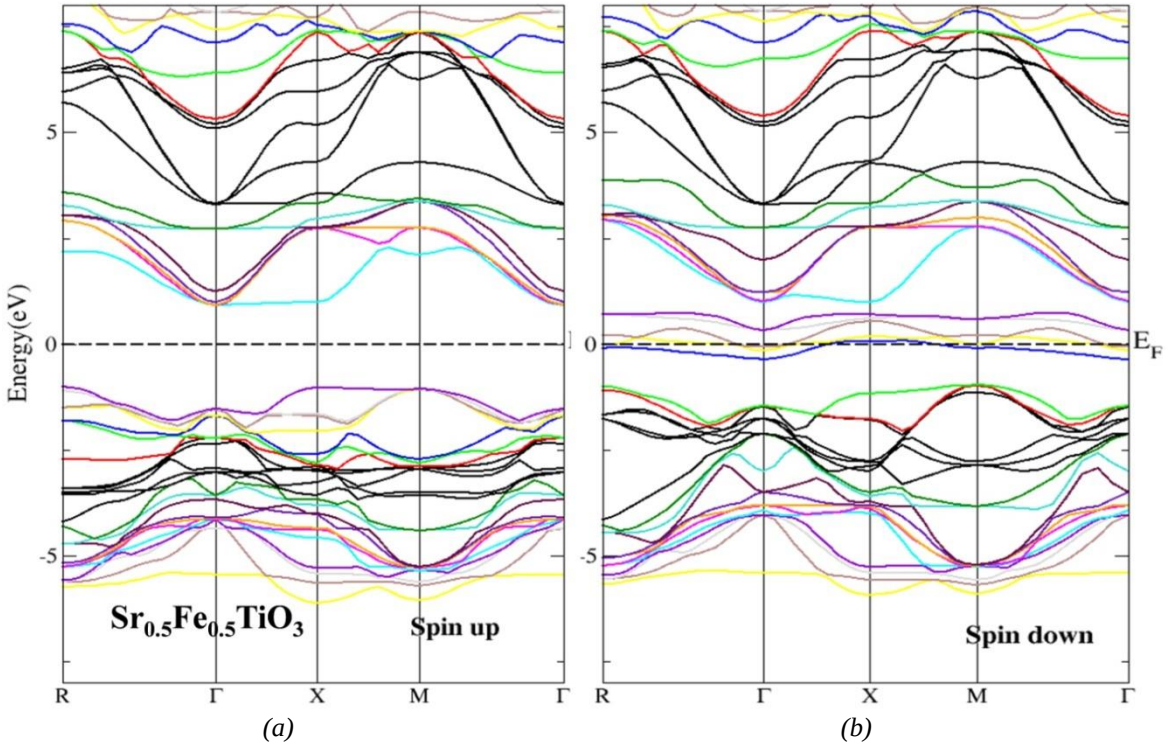

Fig. 3. Spin dependent BS for $Sr_{0.5}Fe_{0.5}TiO_3$ (a) majority spin (b) minority spin.

HMF should be totally spin polarized [34, 35]. Therefore for $Sr_{0.5}Fe_{0.}5TiO_3$the spin polarization is confirmed by the formula $P = \frac{N\downarrow - N\uparrow}{N\downarrow + N\uparrow} \times 100$ (where N↑ and N↓denotes the number of DOS present at E_f). Because in spin down channel the states are present at $E_f$while there is no state present in spin up channel.

For further elucidation about the electronic properties, the plots of total density state (T-DOS) for iron-doped $SrTiO_3$ and partial density state (P-DOS) of Fe, Sr, Ti and O are formed versus energy (eV) as shown in Fig. 5(a-f). In case of up-spin state, it is obvious that the VB is mostly formed of Fe-state together with the intermediate composition from O-states and minute contribution from Ti and Sr orbital electrons in the energy span (-6 eV to -1 eV). The orbital electrons of Fe-*d* have major contribution in the VB from -4.8 to -1 eV with respect to other states for majority spin. There is hybridization exists between the Fe-*d* and O-*p* states in the VB. Around the E_f, there is energy-gap for spin-up state which is responsible of semiconducting nature of compound (see Fig. 5a). The intermixing of Ti-*d* and O-*p* sates exist in the CB of majority spin. In case of down-spin state, the lowermost side of CB has maximum contribution (a major peak) of Fe-*d* state and the admixture of levels exists between Fe-*d* and O-*p* states near the and at the E_f as depicted in Fig. 5(c, f). Same contribution of Ti-*d* state is observed for both spin channels in the higher state of CB. Moreover similar contribution is also observed for Sr-*d* state from 0.9 to 7.9 eV.

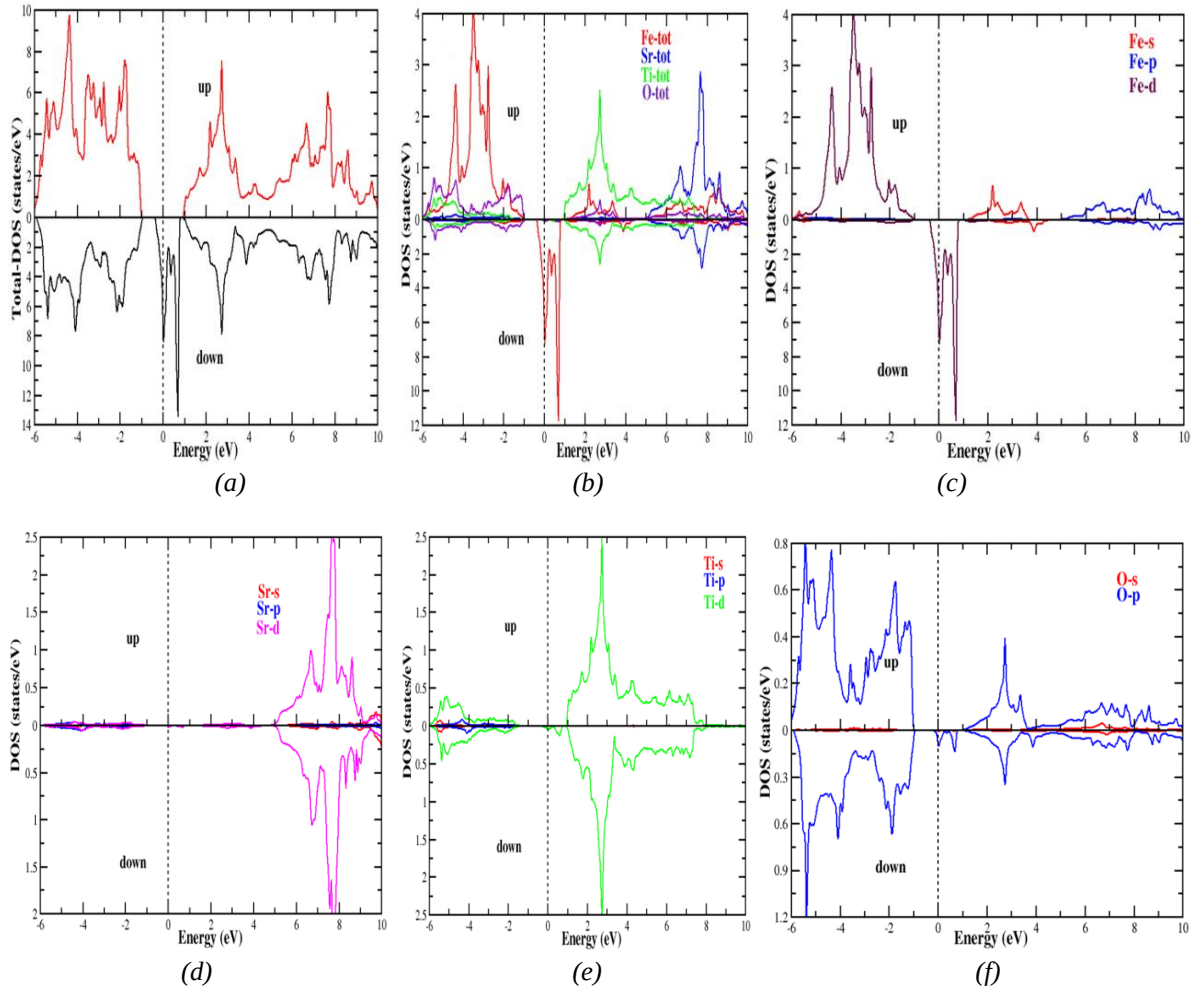

Fig.4. The TDOS and PDOS plots of $Sr_{0.5}Fe_{0.5}TiO_3$ for both spin up and spin down channels.

3.1.2. Electronic properties of $SrTi_{0.5}Fe_{0.5}O_3$

Fig.4 depicts the calculated electronic BS in a highly symmetry lines of the BZ for both spin states of Fe doping at Ti-site in $SrTiO_3$ ($SrTi_{1-x}Fe_xO_3$ (where x = 0.5). It is observed that few VB cross the E_f reach the CB for majority and minority spin channels. This indicates the metallic nature of $SrTi_{0.5}Fe_{0.5}O_3$ due to the same behavior in both spins [11]. The TDOS and PDOS of Iron-doped $SrTiO_3$ compound ($SrTi_{0.5}Fe_{0.5}O_3$) are plotted via energy (eV) as depicted in Fig. 6(a-f). It is observed for up-spin state that the VB is significantly consist of Fe and O states along minute contribution from Ti and Sr orbital electrons from -6 eV to 0 eV. There is strong hybridization exists between the Fe-*d* and O-*p* states below the E_f in the energy range (-1.7 to 0.7 eV) for spin-up channel as depicted in Fig. 6(d, f). The contributions of Ti-*d* and Sr-*d* are almost same for both spin channels in the CB from 1.2-7.9 eV and 4.9-10 eV, respectively. For the down-spin state, it is obvious from Fig.6d that CBM is mainly contributed (prominent peak) by Fe-*d* orbital electrons. There is overlapping of the levels occurs between the Fe-*d* and O-*p* states from -5.1 to 1.9 eV for spin-down state of VB. Moreover, Fe-*d* and O-*p* states are strongly hybridized above the E_f for both spin channels. Basically the transitions of Fe-*d* and O-*p* orbital electrons from VB into CB are responsible for metallic nature of the studied material.

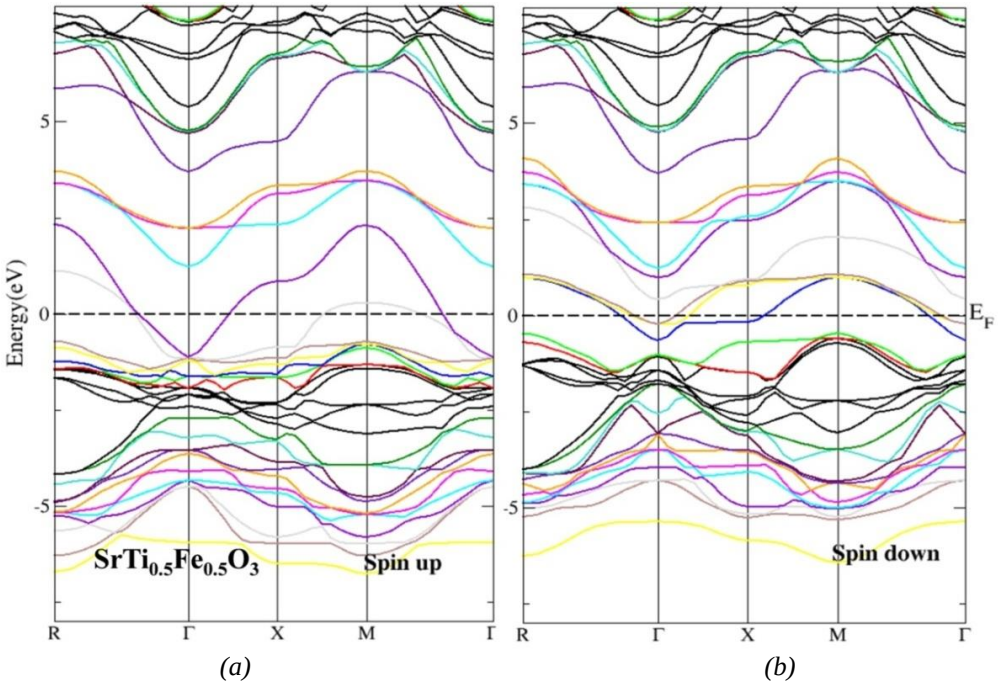

Fig. 5. BS plots for $SrTi_{0.5}Fe_{0.5}O_3$ (a) majority spin (b) minority spin.

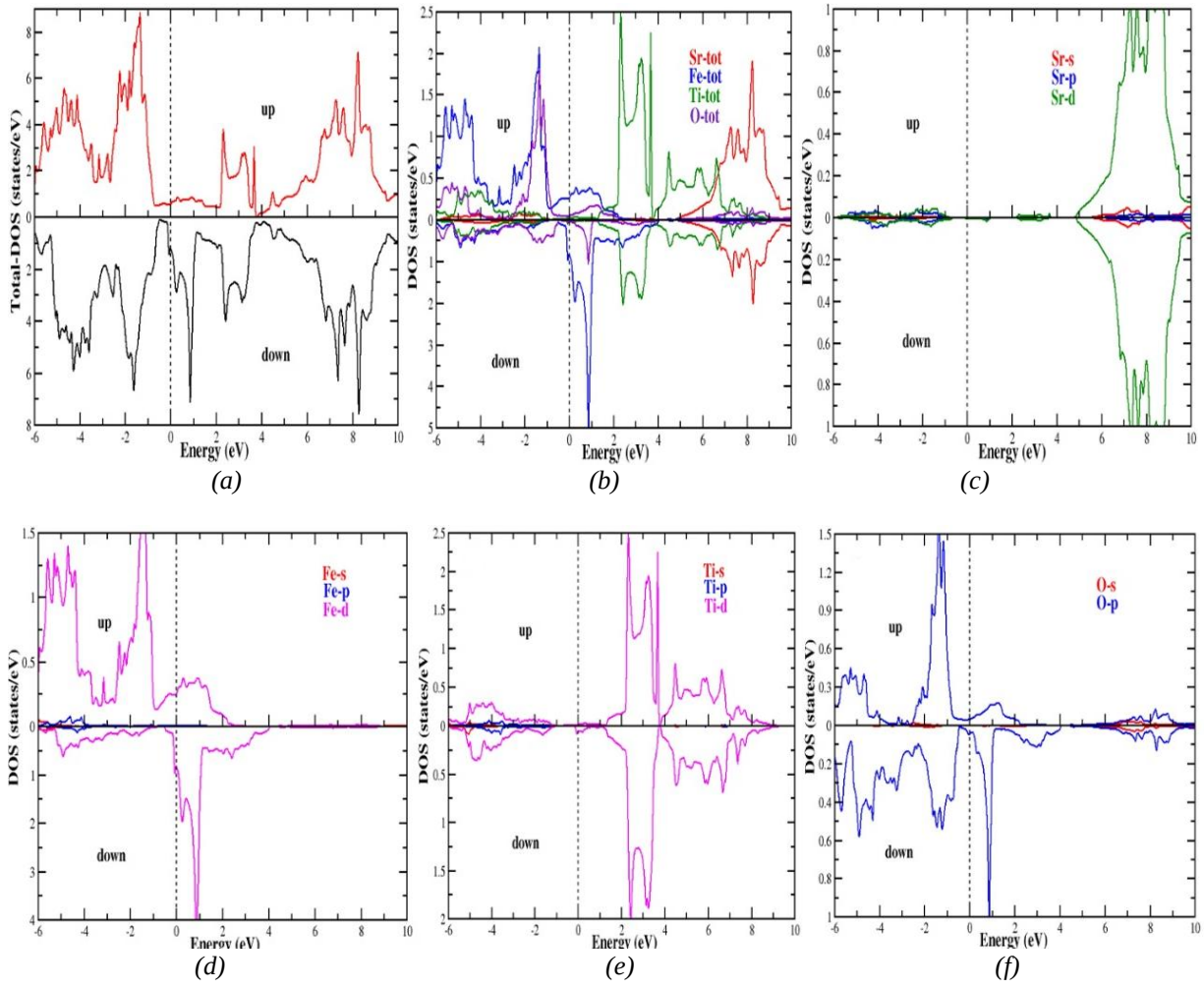

Fig. 6. The TDOS and PDOS plots of $SrTi_{0.5}Fe_{0.5}O_3$ for both spins.

3.2. Magnetic properties

In order to observe the spin effect on the studied materials ($Sr_{0.5}Fe_{0.5}TiO_3$ and $SrTi_{0.5}Fe_{0.5}O_3$), the computed magnetic moments (μ_B) of all atoms that constitutes the material and the interstitial sites are revealed in Table 1. It is noted that the μ_B of dopant atom (Fe) has larger involvement in the total μ_B of the materials. The obtained value of the total μ_B for $Sr_{0.5}Fe_{0.5}TiO_3$ is an integer (4.0002 μ_B) which indicates the characteristic of HMF materials [32, 36]. Whereas the value of total μ_B for $SrTi_{0.5}Fe_{0.5}O_3$ is non-integer (3.5 μ_B) [37] of this compound as presented in Table 1.

Table 1. Computed parameters for $Sr_{0.5}Fe_{0.5}TiO_3$ and $SrTi_{0.5}Fe_{0.5}O_3$ magnetic perovskites in cubic phase.

Properties	$Sr_{0.5}Fe_{0.5}TiO_3$	$SrTi_{0.5}Fe_{0.5}O_3$
a_o(Å)	3.9803	3.980
ε_1 (0)	5.31	14.46
n (0)	26.9	3.84
E_{HM} (eV)	0.914	Metallic
ΔE_C (ev)	-0.574	
ΔE_V (eV)	0.0693	
$N_0\alpha$	-0.00574	
$N_0\beta$	0.00693	
M_{tot}	4.0002	3.5298
M_{Fe}	3.6337	2.8805
M_{Sr}	0.0020	0.0047
M_{Ti}	-0.0083	0.0009
M_O	0.1516	0.2339
M_{Int}	0.0694	0.1708

In case of $Sr_{0.5}Fe_{0.5}TiO_3$, the negative value of the μ_B of Ti atom demonstrates that it is oppositely aligned with the rest of the moments. But for $SrTi_{0.5}Fe_{0.5}O_3$, all μ_B of local atoms and interstitials sites contain a positive signs therefore their moments are aligned parallel with one another. According to Hund's rule, transition metals (TMs) possess μ_B equivalent to the number of unpaired electron present in their valence shell. In $Sr_{0.5}Fe_{0.5}TiO_3$the local μ_B of Fe is slightly reduced whereas in $SrTi_{0.5}Fe_{0.5}O_3$ the Fe μ_B is highly decreased from its free space value ($4\mu_B$) because of the hybridization between *d*-state of Fe and the *p*-state of O in both compounds and generates small local μ_B on other sites. To further explain the ferromagnetic behavior, the knowledge of exchange constants ($N_0\alpha = \Delta E_C$ /x<S>and$N_0\beta = \Delta E_V$ / x<S>) are important. Where ΔE_C and ΔE_V are the conduction and VB edge splitting, x denotes the concentration of dopant and <S> represents half of the total μ_B. These exchange parameters provide information that how VB and CB are affected during the splitting and exchange process. The *s-d* and *p-d* coupling is described by $N_0\alpha$ and $N_0\beta$, respectively.The computed values of $N_0\alpha$, $N_0\beta$, ΔE_C and ΔE_V are presented in table 1. The exchange constant $N_0\alpha$ contains the negative value while exchange constant $N_0\beta$ has positive value. The opposite sign of exchange parameters reveals the antiferromagnetic coupling due to quantum confinement effect [38]. In majority spin channel, the Fe-*d* orbital electrons are above the valance band maxima, and in minority spin channel, the Fe-*d* states are below the minima of CB. Therefore, negative $N_0\alpha$ is a result of kinetic *s-d* interaction [39].

3.2. Optical properties

Interaction of light (photons) with the matter (studied material) is demonstrated by the optical properties which are connected direct with electronic structure of material. Calculations are carried out to discuss the optical characteristics of Iron doped $SrTiO_3$.

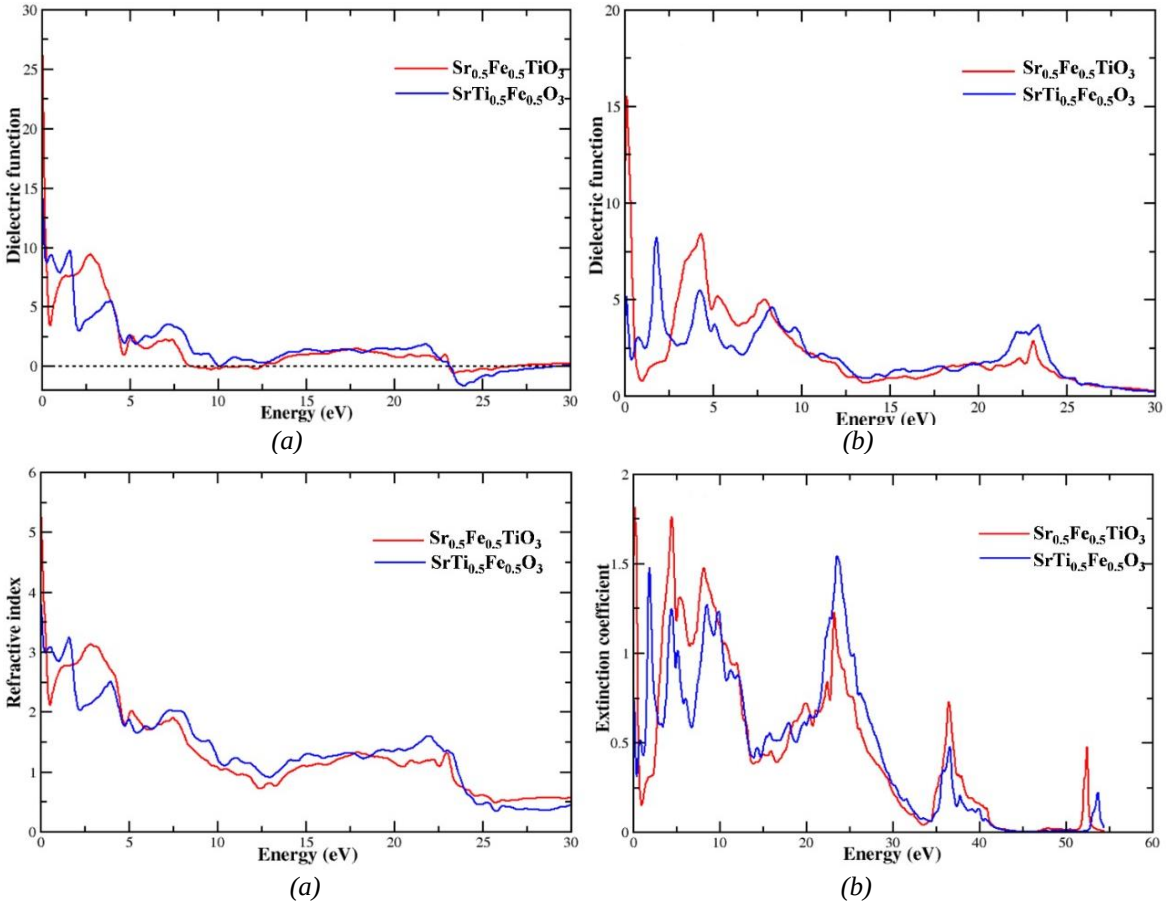

Fig. 7. (a) $\varepsilon_1(\omega)$ *(b)* $\varepsilon_2(\omega)$ *(c)* n (ω*(d)* k (ω *calculated for* $Sr_{0.5}Fe_{0.5}TiO_3$ *and* $SrTi_{0.5}Fe_{0.5}O_3$.

Fig. (7, 8) depicts the comparative plots of various optical constants of Fe doped $SrTiO_3$ versus photon energy (eV) up to 30 eV. The $\varepsilon_1(\omega)$ and $\varepsilon_2(\omega)$ (shown in Fig. 7(a,b)) of DF are computed for $Sr_{0.5}Fe_{0.5}TiO_3$and $SrTi_{0.5}Fe_{0.5}O_3$materials. The observed magnitude of DF at zero frequency $\varepsilon_1(0)$ is 26.9 eV and 14.5 eV for $Sr_{0.5}Fe_{0.5}TiO_3$ and $SrTi_{0.5}Fe_{0.5}O_3$, respectively. The $\varepsilon_1(\omega)$ part reveals the phenomena of polarization as well as dispersion when photons interact with studied compound. There is main peak (first maxima) appeared at 2.7 eV and 9.8 eV for $Sr_{0.5}Fe_{0.5}TiO_3$ and $SrTi_{1-x}Fe_xO_3$, respectively. After that $\varepsilon_1(\omega)$ value start reducing and becomes negative in the energy limit (23.1-25.5 eV) for $Sr_{0.5}Fe_{0.5}TiO_3$ and (23.1-28 eV) for $SrTi_{0.5}Fe_{0.5}O_3$. This indicates that the materials reflect all the incident photons and behave like metal therefore can be employed for protective usage from radiations within this range of energy. The $\varepsilon_2(\omega)$ described the absorption of material and interconnected with BS of the compound [40]. Fig.7b depicts the spectra of $\varepsilon_2(\omega)$, it is clear that the highest absorption (first hump) occur at 3.3 eV and 0.7 eV and second hump (major peak) at 4.2 eV and 1.73 eV for $Sr_{0.5}Fe_{0.5}TiO_3$ and $SrTi_{0.5}Fe_{0.5}O_3$, respectively. This is because of electrons from Fe-*d* (VB) and O-*p* (VB) orbitals make transitions into Ti-d (CB) states in case of $Sr_{0.5}Fe_{0.5}TiO_3$. Whereas Fe-*d* (VB), Ti-*d* (VB) and O-*p* (VB) orbitals electrons into the (Fe, Ti)-*d* and O-*p* states in CB for $SrTi_{0.5}Fe_{0.5}O_3$. Beyond 4.9 eV and 2.3 eV the value of $\varepsilon_2(\omega)$ part goes on reducing after few fluctuations for $Sr_{0.5}Fe_{0.5}TiO_3$ and $SrTi_{0.5}Fe_{0.5}O_3$, respectively. This because of reflection of incident photons by metallic bands.The refractive property is consists of two parts, first is the n (ω) and second is the k (ω). These both parts is related with real $\varepsilon_1(\omega)$ and imaginary $\varepsilon_2(\omega)$ components of DF, respectively and are evaluated through following relations: $n^2-k^2 = \varepsilon_1$ and $2nk = \varepsilon_2$

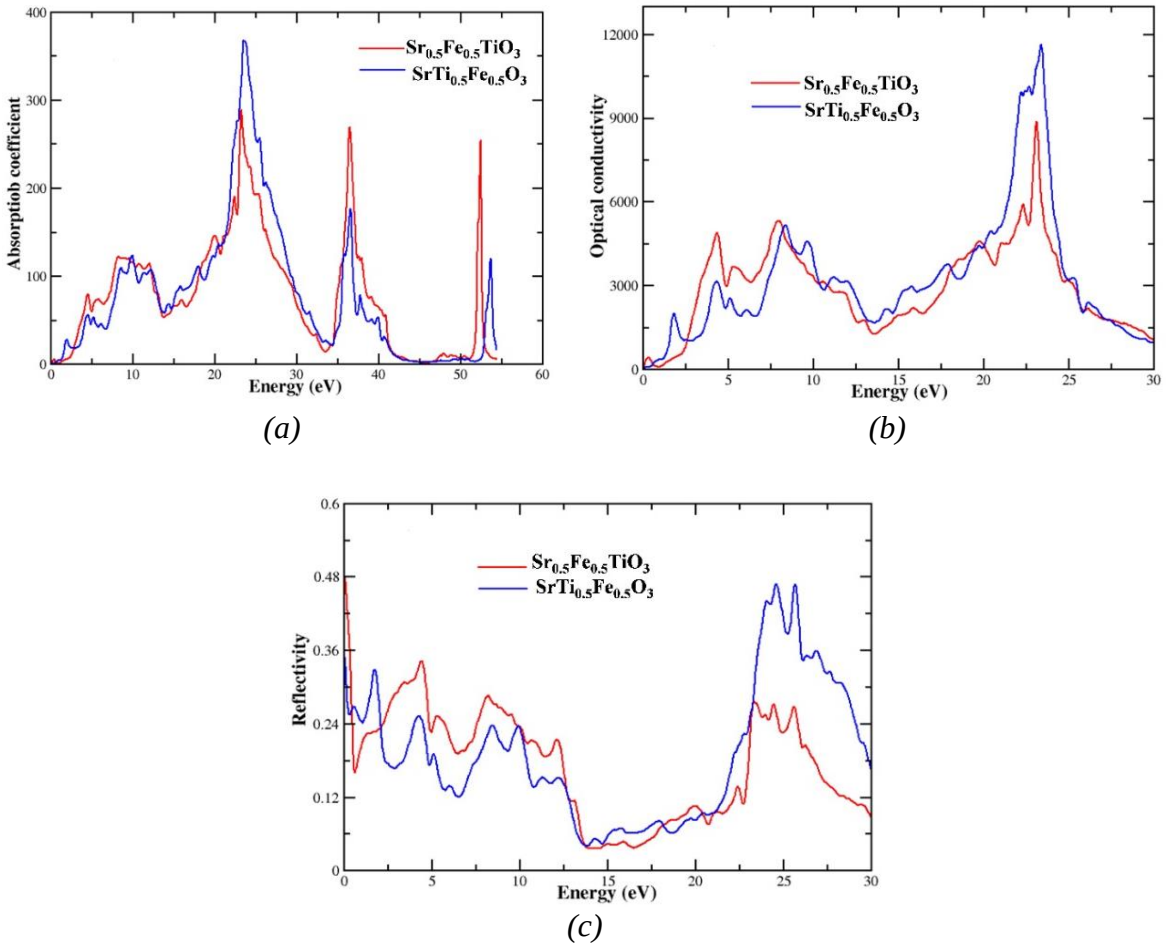

Fig. 8. (a) α (ω) (b) σ (ω)(c) Reflectivity calculated for $Sr_{0.5}Fe_{0.5}TiO_3$ and $SrTi_{0.5}Fe_{0.5}O_3$.

The n (ω) describes the transparent property of studied material (Fe-doped $SrTiO_3$) for incident photons. The value of n (ω at zero energy is attained to be 5.3 eV for $Sr_{0.5}Fe_{0.5}TiO_3$and 3.84eV for $SrTi_{0.5}Fe_{0.5}O_3$. Moreover the static n (0) refractive index equating well with static $\varepsilon_1(0)$ part for $SrTi_{0.5}Fe_{0.5}O_3$by this relation: $n_0^2 = \varepsilon_1$ (0), whereas this relation is not satisfied for $Sr_{0.5}Fe_{0.5}TiO_3$ due to different symmetrical structure. The highest peak of n (ω) observed at 2.7 eV and 1.6 eV, after then its value gradually reduces and becomes less than unity from 11-14 eV, 23.2-30 eV and 12.4-13.2 eV, 23.5-30 eV for $Sr_{0.5}Fe_{0.5}TiO_3$ and $SrTi_{0.5}Fe_{0.5}O_3$, respectively (see Fig.7c). This indicates that V of material becomes higher than the light velocity (c).The k (ω) reveals the similar response as the imaginary DF ε_2 (ω) and describes the attenuating ability of the material for the incident photons [41]. Fig.7d delineate the computed k (ω) spectra, it is observed that the absorption becomes maximum where the value of n (ω) is minimum. The absorption coefficient α (ω) plays a major character in selecting the materials for optoelectronic applications and is associated with band gap of the material [42]. The computed spectra of α (ω) as shown in Fig. 8a, demonstrates that the maximum absorption peak found to be at 23.1 eV and 23.5 eV for $Sr_{0.5}Fe_{0.5}TiO_3$ and $SrTi_{0.5}Fe_{0.5}O_3$, respectively. This value indicates that maximum absorption lies in the UV region of the EM-spectrum. According to this relation a =4πk/λ, the absorption has an inversely related with wavelength of radiation. Therefore, Iron inclusion can be used in engineering the optical features of $SrTiO_3$ in accordance with the requirement. The optical conductivity σ (ω) reveals that when the studied compound absorbed the incident photons, which actuates the free electrons that transfer from VB into CB and causes conductivity. The highest σ (ω) value attained to be 8912.82 Ω^{-1} cm^{-1} at 23.1 eV for $Sr_{0.5}Fe_{0.5}TiO_3$ and 11691.2 Ω^{-1} cm^{-1} at 23.5 eV for $SrTi_{0.5}Fe_{0.5}O_3$shown in Fig. 8b. The R (ω) of the material describes its surface roughness. The spectral behavior of R (ω) is delineated in Fig. 8c. Results indicated that R (ω) gains a large

value where the value of $\varepsilon_1(\omega)$ contains a negative value. The highest value of R (ω) is obtained for $SrTi_{0.5}Fe_{0.5}O_3$ which indicates that this material is used as propitious coating candidate to reduce the solar heating.

4. Conclusions

Physical characteristics of $Sr_{1-x}Fe_xTiO_3$and $SrTi_{1-x}Fe_xO_3$ (where x = 50%) perovskite materials are investigated by performing the first principle calculations. The positive value of $\Delta E = E_{AFM}-E_{FM}$ indicates that studied compounds have more stability in FM phase. The substitution of Fe at A-site in $SrTiO_3$ consequences the HMF character, while the substitution of Fe at B-site in $SrTiO_3$ resulted into metallic character of the studied material. The presence of strong *p-d* hybridization in both $Sr_{0.5}Fe_{0.5}TiO_3$and $SrTi_{0.5}Fe_{0.5}O_3$ generates small μ_B on non-magnetic sites which causes the reduction of Fe-site magnetic moment.

The negative μ_B of Ti atom for $Sr_{0.5}Fe_{0.5}TiO_3$ demonstrates that its moment is oppositely aligned with rest of the non-magnetic sites moments. For $Sr_{0.5}Fe_{0.5}TiO_3$, the computed exchange constants $N_0\alpha$ and $N_0\beta$ possess opposite sign values. In case of $SrTi_{0.5}Fe_{0.5}O_3$, the n(0) and static dielectric constant satisfied the relation $n_0^2 = \varepsilon_1(0)$. The highest absorption lies in the UV region of the EM-spectrum for both the studied compounds. The highest value of R (ω) is obtained for $SrTi_{0.5}Fe_{0.5}O_3$. The reflectivity value is maximum where the real part $\varepsilon_1(\omega)$ contains a negative value. The over analysis demonstrate that $Sr_{0.5}Fe_{0.5}TiO_3$ is prominent candidate in spintronic and optoelectronic technology.

Acknowledgements

1. This research was funded by the Deanship of Scientific Research at Princess Nourah bint Abdulrahman University through the Fast-track Research Funding Program.

2. The author (R. Neffati) extends his appreciation to the Deanship of Scientific Research at King Khalid University, Saudi Arabia for funding this work through Research Groups Program under grant number (R.G.P.2/170/42).

References

[1] D. Zhu, P. Cao, W. Liu, X. Ma, A. Maignan, B. Raveau, Materials Letters **61**,617 (2007).
[2] S.Mubashir, M. K.Butt, M.Yaseen, J.Iqbal, M.Iqbal, A.Murtaza, A.Laref, *Optik* **239**, 166694(2021).
[3]F.Shakoor, S. A.Aldaghfag, M.Yaseen, M. K.Butt, S.Mubashir, J.Iqbal, M. Zahid, A. Murtaza,A.Dahshan, *Chemical Physics Letters*, **779**, 138835(2021).
[4] R.B. Behram, M.A. Iqbal, S.M. Alay-e-Abbas, M. Sajjad, M. Yaseen, M.I. Arshad, G. Murtaza, Materials Science in Semiconductor Processing **41**, 297 (2016).
[5] K.C. Bhamu, A. Dashora, G. Arora, B.L. Ahuja,Radiation Physics and Chemistry**81**, 728 (2012).
[6] S. Hui, A. Petric, Materials Research Bulletin**37**, 1215 (2002).
[7]R.L. Wild, E.M. Rockar, J.C. Smith, Physical Review B**8**, 3828(1973).
[8] J.N. Yun, Z.Y. Zhang, Acta Physico-Chimica Sinica **26**, 751 (2010).
[9] G. Viruthagiri, P. Praveen, S. Mugundan, E. Gopinathan, Indian Journal of Advances in Chemical Science **1**, 132 (2013).
[10] Y. Duan, P. Ohodnicki, B. Chorpening, G. Hackett, Journal of Solid State Chemistry **256**, 239 (2017).
[11] M. Yaseen, H. Ambreen, J. Iqbal, A. Shahzad, R. Zahid, N.A. Kattan, S. M. Ramay, A. Mahmood, *Philosophical Magazine*, **100**(24), 3125-3140 (2020).

Z. Ali, I. Ahmad, I. Khan, B. Amin, Intermetallics **31**, 287 (2012).
[12] H.W. Kang, S.B. Park, Chemical Engineering Science **100**, 384 (2013)
[13] C.M. Liu, X. Xiang, X.T. Zu, Chinese Journal of Physics **47**,893 (2009)
[14] A.G. Şale, S. Kazan, J.I. Gatiiatova, V.F. Valeev, R.I. Khaibullin, F.A. Mikailzade, Materials Research Bulletin **48**, 2861 (2013).
[15] L.F. Da Silva, J.C. M'Peko, J. Andres, A. Beltran, L. Gracia, M.I. Bernardi, A. Mesquita, E. Antonelli, M.L. Moreira, V.R. Mastelaro, The Journal of Physical Chemistry C**118**, 4930 (2014).
[16] W. Luo, W. Duan, S.G. Louie, M.L. Cohen, Physical Review B**70**, 214109 (2004).
[17] C. Zhang, Y. Jia, Y. Jing, Y. Yao, J. Ma, J. Sun, Computational Materials Science **79**, 69 (2013).
[18] M. Rizwan, A. Ali, Z. Usman, N.R. Khalid, H.B. Jin, C.B. Cao, Physica B: Condensed Matter **552**, 52 (2019).
[19] T. Shen, C. Hu, H.L. Dai, W.L. Yang, H.C. Liu, C.L. Tan, X.L. Wei, Optik**127**, 3055 (2016).
[20] C. Zhang, Y. Jia, Y. Jing, Y. Yao, J. Ma, J. Sun, Physica B: Condensed Matter**407**, 4649 (2012).
[21] X.G. Guo, X.S. Chen, W. Lu, Optik**126**, 441 (2003).
[22] D. Wang, J. Ye, T. Kako, T. Kimura, The Journal of Physical Chemistry B**110**, 15824 (2006).
[23] H.S. Arif, G. Murtaza, H. Hanif, H.S. Ali, M. Yaseen, N.R. Khalid, Journal of Environmental Chemical Engineering **5**, 3844 (2017).
[24] W. Zhang, H.P. Li, W. Pan, Key Engineering Materials**512**, 1438 (2012).
[25] N. Maikhuri, A.K. Panwar, A.K. Jha, Journal of Applied Physics **113**, 17D915 (2013).
[26] E. Sjöstedt, L. Nordström, D.J. Singh, Solid State Communications **114**, 5 (2000).
[27] K. Schwarz, P. Blaha, Electronic structure of solids and surfaces with WIEN2k, In Practical aspects of computational chemistry I, Springer, Dordrecht, (2011).
[28] J.P. Perdew, K. Burke, M. Ernzerhof, Physical Review Letters **77**, 3865 (1996).
[29] P.E. Blöchl, O. Jepsen, O.K. Andersen, Physical Review B**49**, 16223 (1994).
[30] H. Ehrenreich, M.H. Cohen, Physical Review **115**, 786 (1959).
[31] S. Cottenier, Instituutvoor Kern-enStralingsfysica, KU Leuven, Belgium**4**, 41 (2002).
[32] W. Tanveer, Q. Mahmood, M.A. Faridi, M. Yaseen, S.M. Ramay, A. Mahmood, Journal of Superconductivity and Novel Magnetism **30**, 3481 (2017).
[33] R.A. De Groot, F.M. Mueller, P.G. Van Engen, K.H.J. Buschow, Physical Review Letters **50**, 2024 (1983).
[34] Q. Mahmood, S.M. Alay-e-Abbas, A. Mahmood, M. Yaseen, I. Mahmood, N.A. Noor, J. Supercond. Nov. Magn. **29**, 521 (2016).
[35] M. K. Butt, Yaseen, M., Iqbal, J., Altowyan, A. Murtaza, M. Iqbal, A. Laref, *Journal of Physics and Chemistry of Solids*, **154**, (2021).
[36] M. Yaseen, H. Ambreen, U. Shoukat, M. Butt, S. Noreen, S. Rehman, S. Ramay, Journal of Ovonic Research **15**,401 (2019).
[37] M.K.Butt, M.Yaseen, A.Ghaffar, M.Zahid. *Arabian Journal for Science and Engineering*, **45**(6), 4967-4974 (2020).
S. Ali, W. Khan, G. Murtaza, M. Yaseen, S.M. Ramay, A. Mahmood, Journal of Magnetism and Magnetic Materials **441**, 113 (2017).
[38] S. Nazir, N. Ikram, S.A. Siddiqi, Y. Saeed, A. Shaukat, A.H. Reshak, Current Opinion in Solid State & Materials Science **14**, 1 (2010).
[39] G.M. Dalpian, S.H. Wei, Physical Review B**73**, 245204 (2006).
[40] Q. Mahmood, M. Yaseen, M. Hassan, S.M. Ramay, A. Mahmood, Chinese Physics B**26**, 087803 (2017).
[41] B. Modak, K. Srinivasu, S.K. Ghosh, RSC Advances **4**, 45703 (2014).
[42] S.Riaz, M.Yaseen, M.K.Butt, S.Mubashir, J.Iqbal, A.S.Altowyan,A. Dahshan,A.Murtaza,M. Iqbal, A.Laref, *Materials Science in Semiconductor Processing*, **133**, 105976 (2021).
[43] M. Yaseen, M. K. Butt, A. Ashfaq, J. Iqbal, M. M. Almoneef, M. Iqbal, A. Murtaza, A. Laref, *Journal of Materials Research and Technology*, **11**, 2106-2113 (2021).